FAULT AND JOINT MEASUREMENTS IN AUSTIN CHALK, SUPERCONDUCTING SUPER COLLIDER SITE, TEXAS

Topical Report

by

H. S. Nance, S. E. Laubach, and A. R. Dutton

Prepared for

Texas National Research Laboratory Commission

under Contract No. IAC(92-93)-0301

Bureau of Economic Geology

The University of Texas at Austin

Box X, University Station

Austin, Texas 78713-7508

June 1994

Contents

Figures

Tables

ABSTRACT

Structure maps of 9.4 mi of nearly continuous tunnel excavations and more than 10 mi of other exposures and excavations in Austin Chalk at the Superconducting Super Collider (SSC) site in Ellis County, Texas, record normal-fault and joint populations in the subsurface within the northern segment of the Balcones Fault Zone that has unmatched resolution for such a long traverse. Small faults (<10 ft throw) occur in clusters or swarms that have as many as 24 faults. Fault swarms are as much as 2,000 ft wide, and spacing between swarms ranges from 800 to 2,000 ft, averaging about 1,000 ft. Predominantly northeast-trending joints are in swarms spaced 500 to more than 21,000 ft apart.

UNRIVALED VIEW OF A FAULT ZONE

Faults and joints are conduits for ground-water flow and targets for horizontal drilling in the petroleum industry. Yet spacing and size distribution of faults and joints in regional fault zones are rarely predicted accurately by current structural models or documented adequately by conventional borehole or outcrop samples. Tunnel excavations present opportunities to measure fracture attributes in continuous subsurface exposures. These measurements can be used to improve structural models and guide interpretation of conventional borehole and outcrop data.

Tunnel excavations for the Superconducting Super Collider (SSC) in Ellis County, Texas (Figs. 1 and 2), provide a view of faults and fractures in a subsurface traverse that is unmatched for length within a regional fault zone. Maps of 9.4 mi of nearly continuous tunnels record geographic distribution and descriptive information for faults and joints. Mapping was undertaken to provide data needed for modeling ground-water flow and monitoring water levels at the site. This paper describes tunnel conditions and mapping procedures, types of fracture information recorded on maps, and preliminary results.

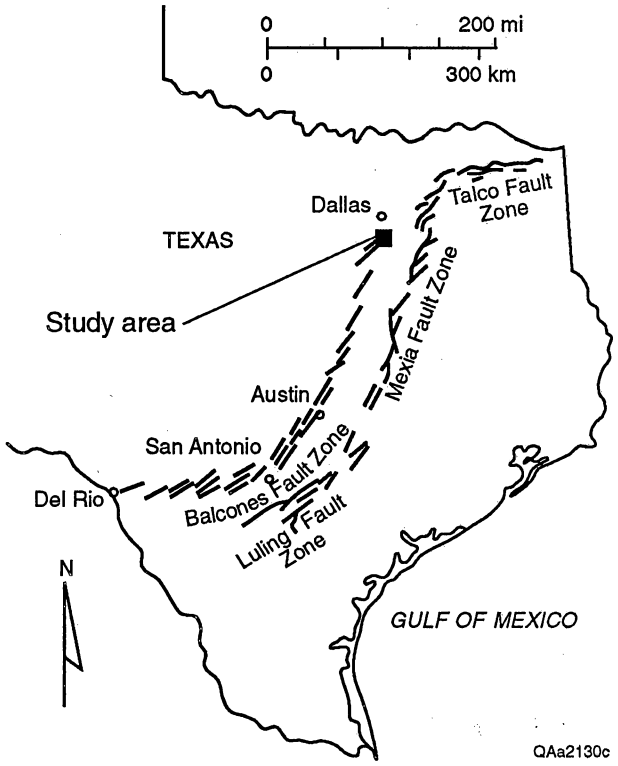

Figure 1. Map of Texas showing SSC site and major Gulf Coast Basin normal fault zones, including Balcones Fault Zone.

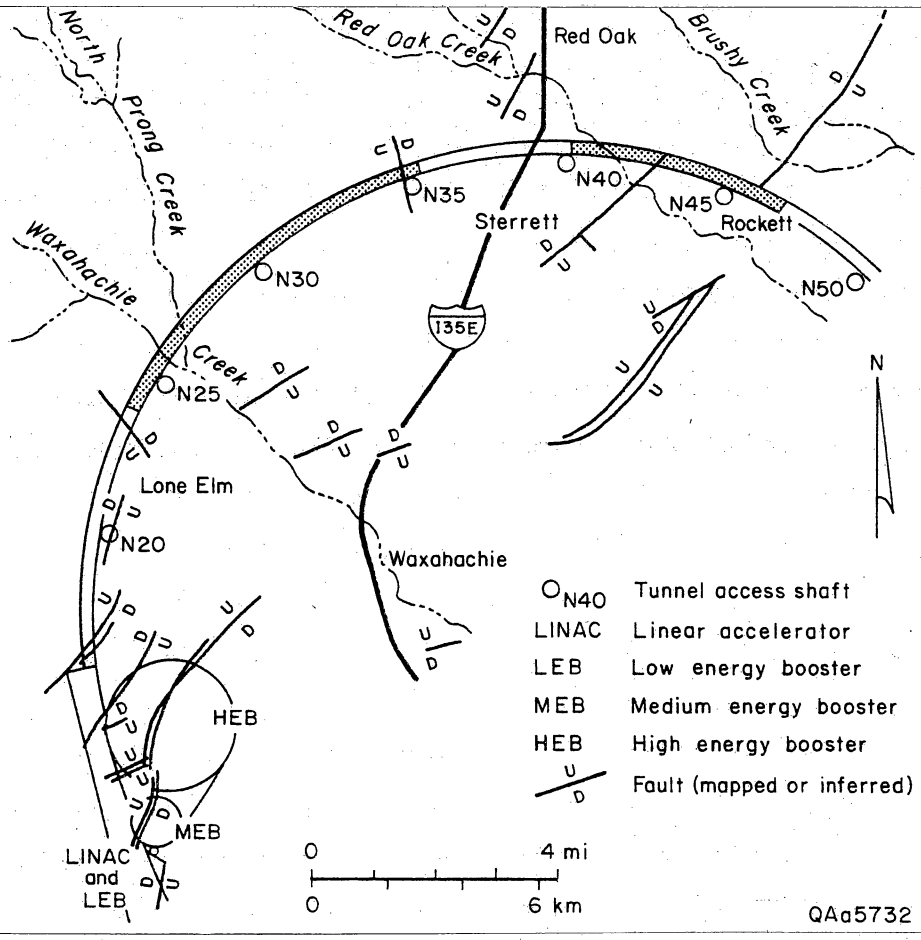

Figure 2. Map of SSC site near Waxahachie, Texas, showing mapped tunnel segments (shaded area) and major faults (throws >20 ft).

SUPERCONDUCTING SUPER COLLIDER (SSC) SITE

The SSC was to be a state-of-the-art particle accelerator, having a design that called for a racetrack-shaped tunnel 54 mi in circumference. The excavated tunnels are about 14 to 16 ft in diameter at an average depth of 150 ft below ground surface (Gilchriese and Metropolis, 1990). In addition to the tunnel, SSC plans included excavations for subsidiary booster rings and experimental halls. Although construction was terminated in 1993, more than 14 mi of tunnels and shafts, as well as numerous open excavations, were completed in Austin Chalk, lower Taylor Marl, and Eagle Ford Shale. The plane of the SSC ring inclines to the southeast at an angle slightly less than the regional dip of Cretaceous strata. The southeastern side of the ring was to have been at depths of as much as 220 ft. Most completed excavations and tunnel segments are on the northwestern side of the ring, at depths of 35 to 200 ft.

SCOPE OF MAPPING

Surface and tunnel excavations at the SSC site expose parts of the Balcones Fault Zone (Fig. 1) along a discontinuous arc that extends 14.2 mi along the fault zone's regional strike and 5.7 mi across regional strike. Tunnel maps show chalk and marl stratigraphy and the location and attitude of folds, faults, and joints. Inch- to yard-thick chalk and marl marker beds allow accurate documentation of fault throw for faults with throws <16 ft. Information recorded for each fault and joint includes the shape, size, and distribution of fracture-fill minerals, breccia, and marl smears. Notes on field maps qualitatively track changes in water discharge from fractures over a six-month monitoring period. Areas of marked construction-related damage or areas covered by shotcrete are also indicated.

SSC GEOLOGY

Austin Chalk

Four SSC tunnel segments, totaling 9.4 mi in length, were excavated in Upper Cretaceous Austin Chalk. Austin Chalk is exposed in a long, narrow belt that is parallel to the Gulf Coast Basin margin (McGowen et al., 1987). In Ellis County, the unit ranges from 430 to 500 ft thick (Collins et al., 1992). In SSC excavations, principal units exposed are lower and middle members of the Austin Chalk (units T to E of Collins et al., 1992). Chalk is overlain by the Ozan Formation (lower Taylor Marl) and underlain by the Eagle Ford Shale, both of Late Cretaceous age.

Austin Chalk is an open-marine foraminifer- and coccolith-bearing limestone arranged in 3- to 6-ft-thick chalk and marl couplets (Hovorka and Nance, in press). Chalk beds are composed of partly fragmented nannoplankton matrix having 5 to 25 percent foraminifers and whole and fragmented inoceramid pelecypods, as well as other sparse fauna. Beds are light gray in the subsurface and have been intensely burrowed. Marl beds consist of varying mixtures of nannoplankton chalk, siliciclastic detritus, authigenic clay, and organic material. Marl beds contain 12 to 40 percent clay and as much as 3.5 percent organic carbon mixed with chalk, giving them a dark color. Marl beds are also burrowed, although lamination is preserved in some beds. Locally, marl beds are bentonitic, recording Late Cretaceous volcanic activity. In tunnel exposures, chalk beds are 0.5 to 6.5 ft thick. Marl beds are 1 inch to about 1 ft thick. Austin Chalk commonly has low matrix permeability (0.03 to 1.27 md) and porosity that ranges from 18.8 to 34.5 percent (S. D. Hovorka, Bureau of Economic Geology, personal communication, 1994).

Balcones Fault Zone

The SSC site lies at the northern end of the Balcones Fault Zone, which extends from near Dallas southward beyond San Antonio (Fig. 1). The Balcones Fault Zone is one of several normal fault zones that rim the Gulf Coast Basin. Movement in this zone occurred predominantly during the Tertiary (Collins and Laubach, 1990). The fault zone marks gulfward tectonic extension, flexure, and tilting along the Gulf Coast Basin perimeter. Tilt is reflected in regional easterly dip changes of 10 to 100 ft/mi across the fault zone. Structural relief across the 10- to 15-mi-wide outcrop belt in Ellis County is about 1,000 ft.

Near the SSC site, large faults mapped on the basis of surface exposures and borehole data have throws of 20 to 100 ft (Reaser and Collins, 1988) (Fig. 2). Tunnels N20–N35+ are north and west of mapped major northeast-trending Balcones faults (Fig. 2). If additional unmapped major northeast-trending faults do not occur to the west of those mapped, then tunnel faults in these segments occur outside of grabens bounded by the major faults. Fault and joint strikes are oriented predominantly northeastward, but northwest-striking faults are prevalent subsidiary elements of the pattern. Commonly, major faults in the area bound narrow, slightly asymmetric grabens. In outcrop, major faults generally have steep dips (60°–70°) and are planar, but minor faults having curved and undulatory shapes in plan view and cross section are common (Collins et al., 1992). Faults with less than 5 ft of throw are the most common fracture type seen in core (Collins et al., 1992). Seismic and well data have been thought to show that some large faults flatten and die out within Eagle Ford Shale (The Earth Technology Corporation, 1989).

Outcrop joint studies and 99 shallow vertical and slant cores in the 300-mi^2 area surrounding the SSC site demonstrated that two joint regimes are present (Collins et al., 1992): (1) a highly fractured, weathered horizon typified by orthogonal and polygonal joint-trace patterns and (2) an underlying less fractured, unweathered zone having widely spaced planar, vertical joints and veins. In the least weathered outcrops, northeast-striking joints are locally arranged in widely spaced swarms rather than being evenly spaced. Although outcrops of

individual beds are rarely long enough to accurately assess spacing patterns, distances between fracture swarms of as much as several hundred feet have been documented (Collins et al., 1992).

TUNNEL EXCAVATION

SSC tunnels were excavated by tunnel boring machines (TBMs), which are devices that advance "inchworm" style in 5- to 6-ft increments by bracing themselves on tunnel walls with diametrically extended hydraulic sidewall grippers. A separate longitudinal hydraulic system acts to thrust a rotating cutting head forward. The cutter head is fixed with tools, and a circular rock face is chipped. The final step in an advance cycle is to retract the gripper pads, drawing the rear part of the device forward (Nelson, 1993). In Austin Chalk, boring with TBMs resulted in a smooth, nearly damage free tunnel surface that is ideal for preserving fine details of structure.

In SSC tunnels, TBMs advanced as much as 450 ft/day (Jim Carroll, SSC Laboratory, personal communication, 1994). The tunnel was excavated in segments accessed by vertical shafts 30 or 50 ft in diameter labeled N25, N30, and so forth. Shafts are used as reference points in our description (Fig. 2). For example, N25–N30 refers to the tunnel segment between access shafts N25 and N30; segment N40–N45.3 extends one-third the distance toward N50 from N45; and N30–N35+ extends a few hundred feet toward N40 from N35.

Chalk dust and muck (moist mined rock chips) produced by tunnel boring mostly obscure the lower half of the tunnel. Best exposures are in tunnel segment N25–N30, which was cleaned with high-pressure water spray. Precast concrete floor inserts (invert segments) cover tunnel floors (~60° of the tunnel surface). In 700 ft of tunnel segment N25–N30, exposed geology was covered with spray-applied concrete (shotcrete). Concrete-lined tunnels in Eagle Ford Shale (most of N15–N25) or Taylor Marl were also unmapped.

FRACTURE DATA

Map Methods

Structural and stratigraphic information was recorded on 1:1,200-scale topographic maps prepared by SSC design engineers and on 1:120-scale map forms keyed to tunnel survey marks (Fig. 3a). Survey marks, accurate to the nearest 1 ft, provided location coordinates along the tunnel. Features are located on map forms having a ±1-ft margin of error (Nance, 1993). From tunnel coordinates, strike was measured by reference to tunnel-design maps. Dip was calculated using three accurately located points on inclined surfaces. Fault and joint orientation data are given in Appendices A and B, respectively. Standard measurement methods were used at ground surface, including steel tape measure, pocket transit, and topographic site maps. However, it was impossible to make reliable magnetic measurements in most tunnel segments because steel rails, heavy steel conveyor systems, and steel plumbing were present.

The projection used as a base map for fracture maps is an unwrapped image of the tunnel wall, with tunnel crown at 12 o'clock, springlines (midheight) at 3 o'clock and 9 o'clock, and center of floor (invert) at 6 o'clock (Fig. 3a). This projection is similar to that of borehole-imaging geophysical logs such as the borehole televiewer used to characterize fractures in petroleum wells (for example, Laubach et al., 1990). Other areas of the form were used to illustrate structural aspects not readily mappable on the grid.

During the course of mapping, field data were transferred to vertically exaggerated (50×) cross sections constructed as projections onto an imaginary plane located along tunnel centerline (Fig. 4). Specific structural features were photographed.

Tunnel Conditions

Tunnel segments were visited several times during construction to monitor water inflow and to take advantage of the way changing tunnel conditions highlight different geologic

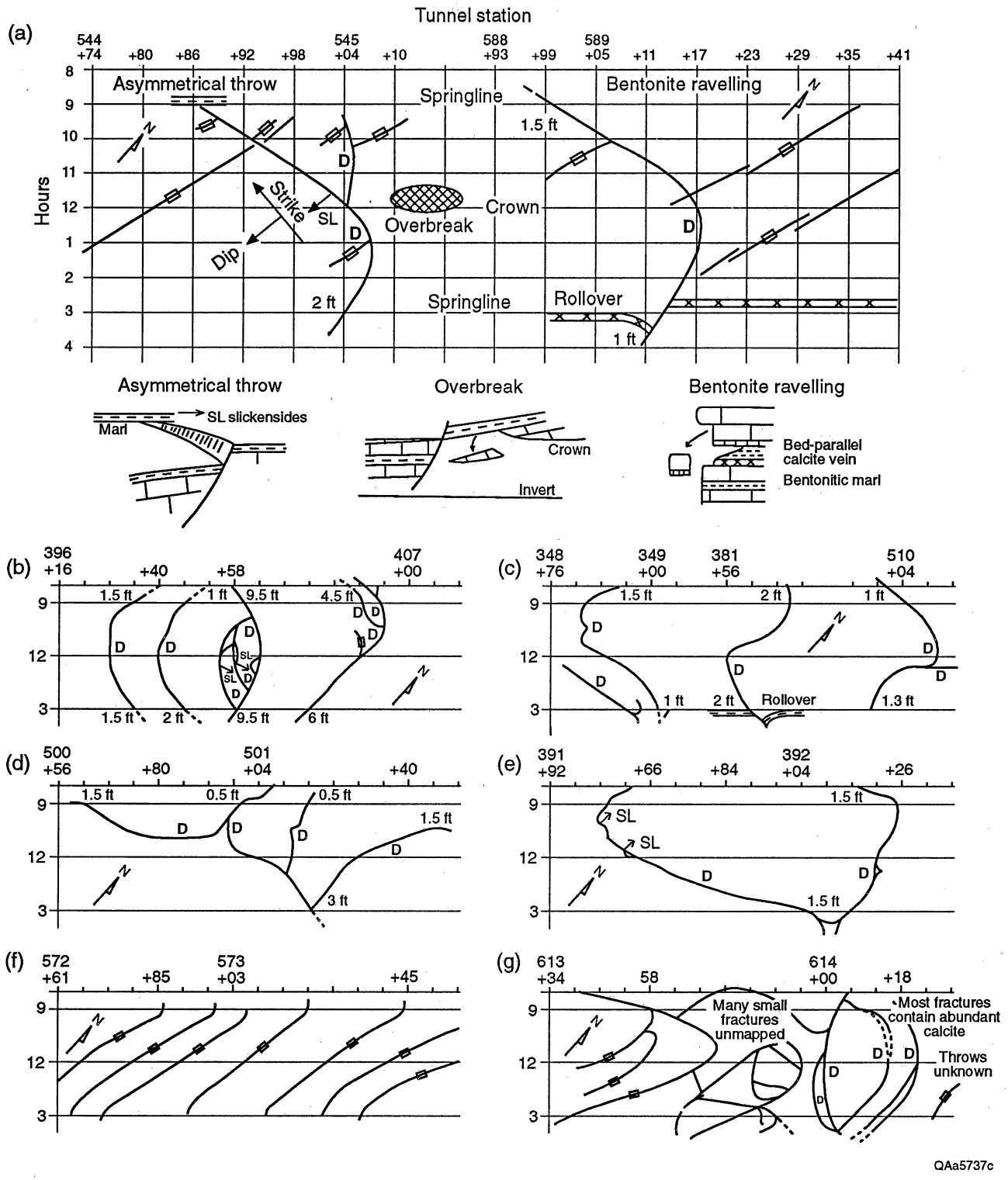

Figure 3. Examples of fault patterns on tunnel maps: (a) map form showing how features are represented on field maps, (b) graben with antithetic faults and fault-bounded lens, (c) curviplanar faults and rollover monocline on hanging wall of central fault, (d) faults ending against other faults, (e) graben, (f) joint swarm, and (g) association of faults and joints near N35 in major fault zone (estimated throw 70 ft).

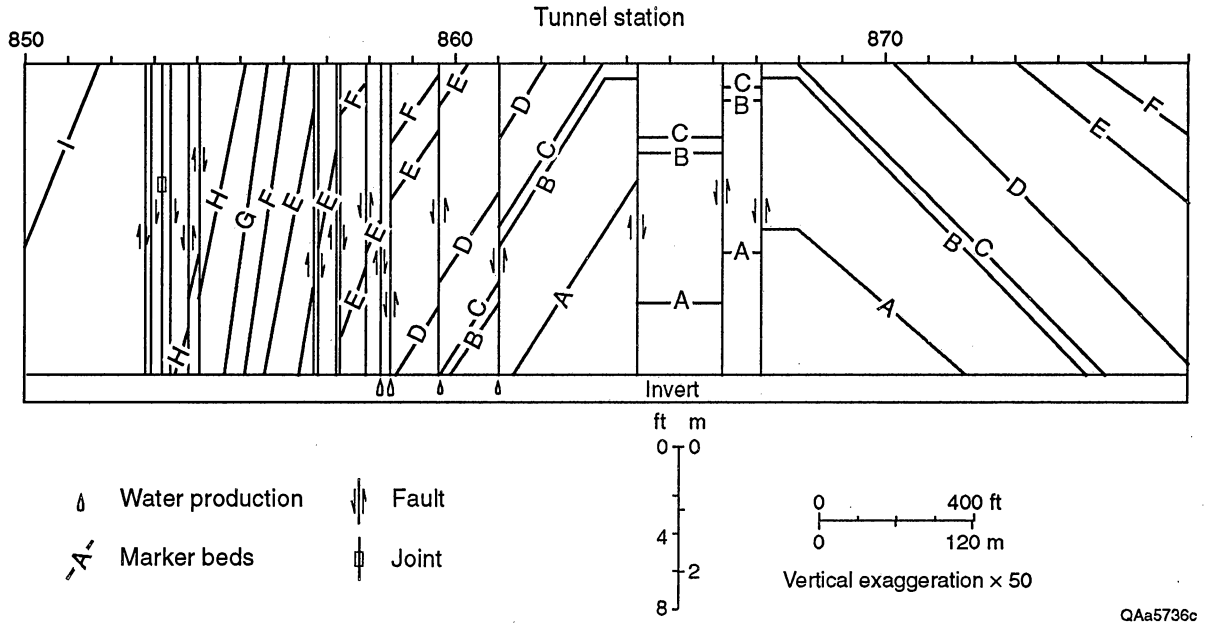

Figure 4. Example of tunnel cross section (wall map exposures projected to plane of tunnel vertical centerline) showing faulted anticline in N40–N45.

Table 1. Stratigraphic levels, excavation conditions, and visible features of the mapped SSC site.

Location	Length (mi)	Interval	Excavation condition	Visible features
N20–N25	2.7	Eagle Ford Shale, lower Austin Chalk	92 percent covered, chalk partly cleaned	Rock types, fracture attributes
N25–N30	2.7	lower Austin Chalk	95 percent exposed, thoroughly cleaned, painted	Rock types, bed thicknesses, fracture attributes
N30–N35+	2.8	lower Austin Chalk	100 percent exposed, partly cleaned	Rock types, bed thicknesses, fracture attributes
N40–N45.3	3.6	middle Austin Chalk	uncleaned	Strikes, dips, bed attitudes; marker beds traceable for only few hundred feet
LINAC, LEB, MEB, Boz Creek		lower Austin Chalk	cleaned	Rock types, bed thicknesses, fracture attributes

features. Fault zone fracture porosity and water-flow patterns are clearest (or least disturbed) shortly after passage of TBMs, and the presence of closely spaced survey marks allowed the most accurate location measurements. Tunnel plumbing was eventually removed in some areas, and these walls were cleaned thoroughly. Stratigraphic features and fault geometry, as well as locations of joints and small faults, are most readily mapped after wall cleaning. But by this stage of construction a few fault zones had been covered by shotcrete, and most location coordinates were obscured. One tunnel segment (N25–N30) was covered with latex paint to inhibit moisture damage. Despite the paint, the rock type, bed thickness, and fracture attributes are generally visible. When work on the project ceased, tunnel segments were in various stages of completion and discernible geologic features varied among segments (Table 1).

Construction-related tunnel damage (overbreak or rock fallout) consisted mainly of loosened blocks defined by marl beds, natural fractures, and fractures induced by TBM gripper pads. Marl beds within several inches of crown (Fig. 3a) and fractures at low angles to tunnel walls are principal causes of rock fall. Overbreak or fallout makes up less than 1 percent of the tunnel except in areas of bentonite or large fault zones. Wall damage is most prevalent where fault offsets are more than 3 ft and fault breccia and fracture permeability are present. Failure is facilitated by fracture and breccia zones and the presence of fluids within them. If left unprotected from humidity and temperature variations, rock containing expansive clays (for example, bentonite) can expand and/or contract, which leads to damage (Fig. 3a). For example, expansion and/or contraction of a 120-ft-long exposure of bentonite within N30–N35+ caused tunnel damage.

ATTRIBUTES OF FAULTS AND JOINTS

Fractures in SSC tunnels are mostly small (throw <5 ft) planar to curviplanar normal faults or subvertical planar joints (Fig. 5). Fracture orientation and intensity patterns are summarized in Figures 6 and 7 and Table 2. Some attributes of faults and joints in SSC tunnels closely resemble those described from Austin Chalk outcrops (for example, Collins, 1987; Collins et al.,

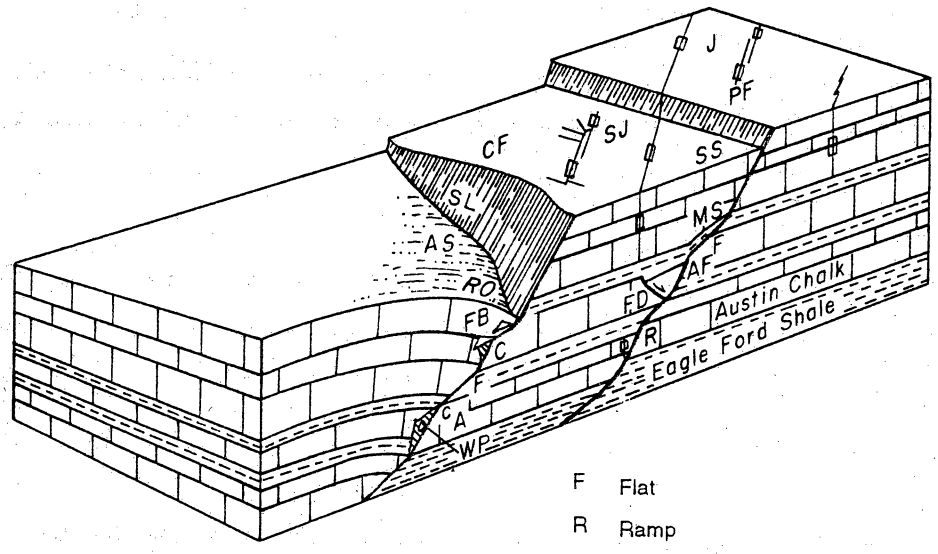

Figure 5. Block diagram summarizing features visible in SSC excavations. No scale.

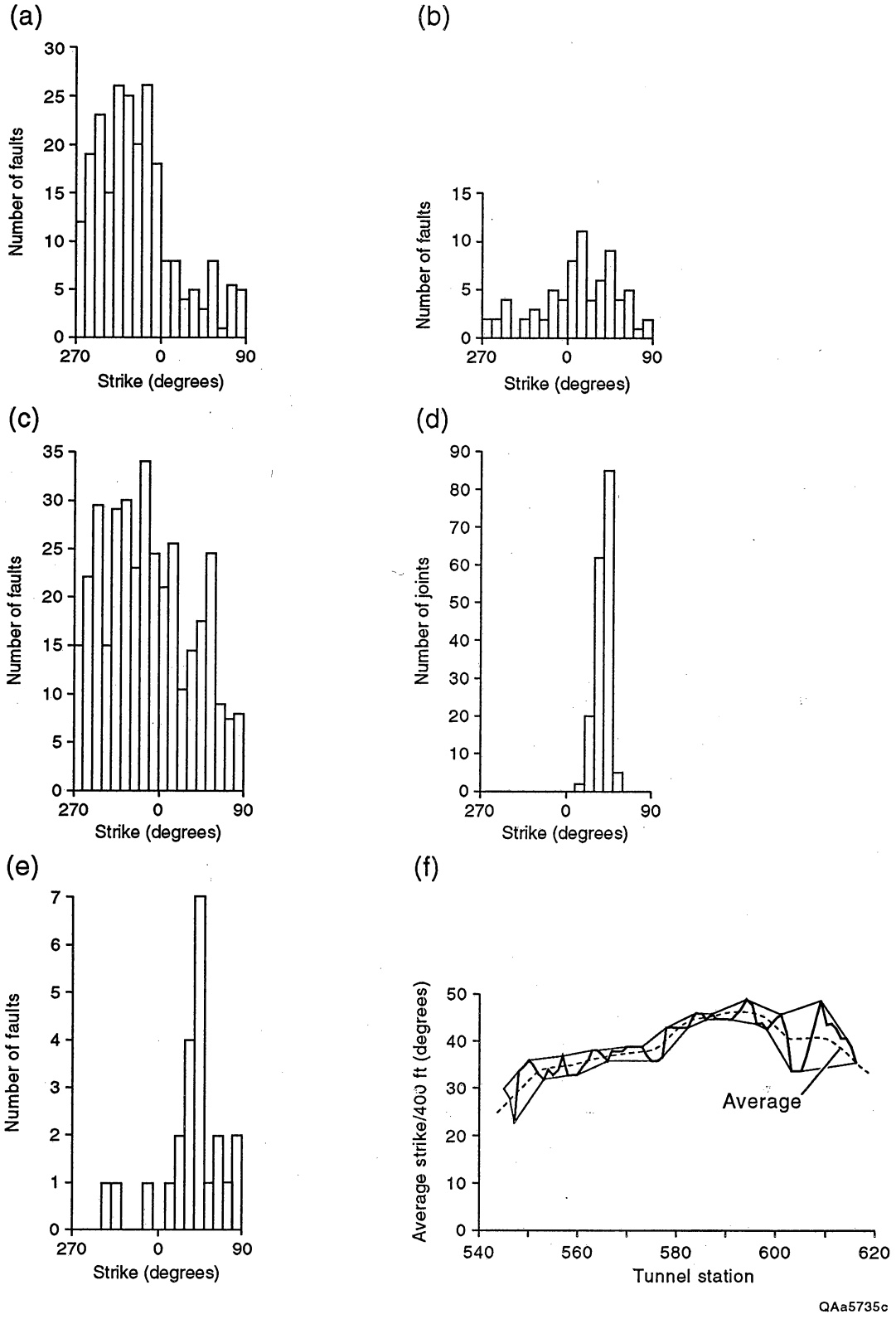

Figure 6. Strike-frequency diagrams for (a) faults in N20–N35+, (b) faults in N40–N45.3, (c) composite of faults in N20–N45.3 (to correct for shorter tunnel length, measurements from N40–N45.3 were multiplied by 1.61), (d) joints in N30–N35+, (e) major faults (throw >20 ft), (f) distribution of joint strikes along N30–N35+ on the basis of 400-ft running average over 7,000 ft; note change in average strike and periodic variance of average strike.

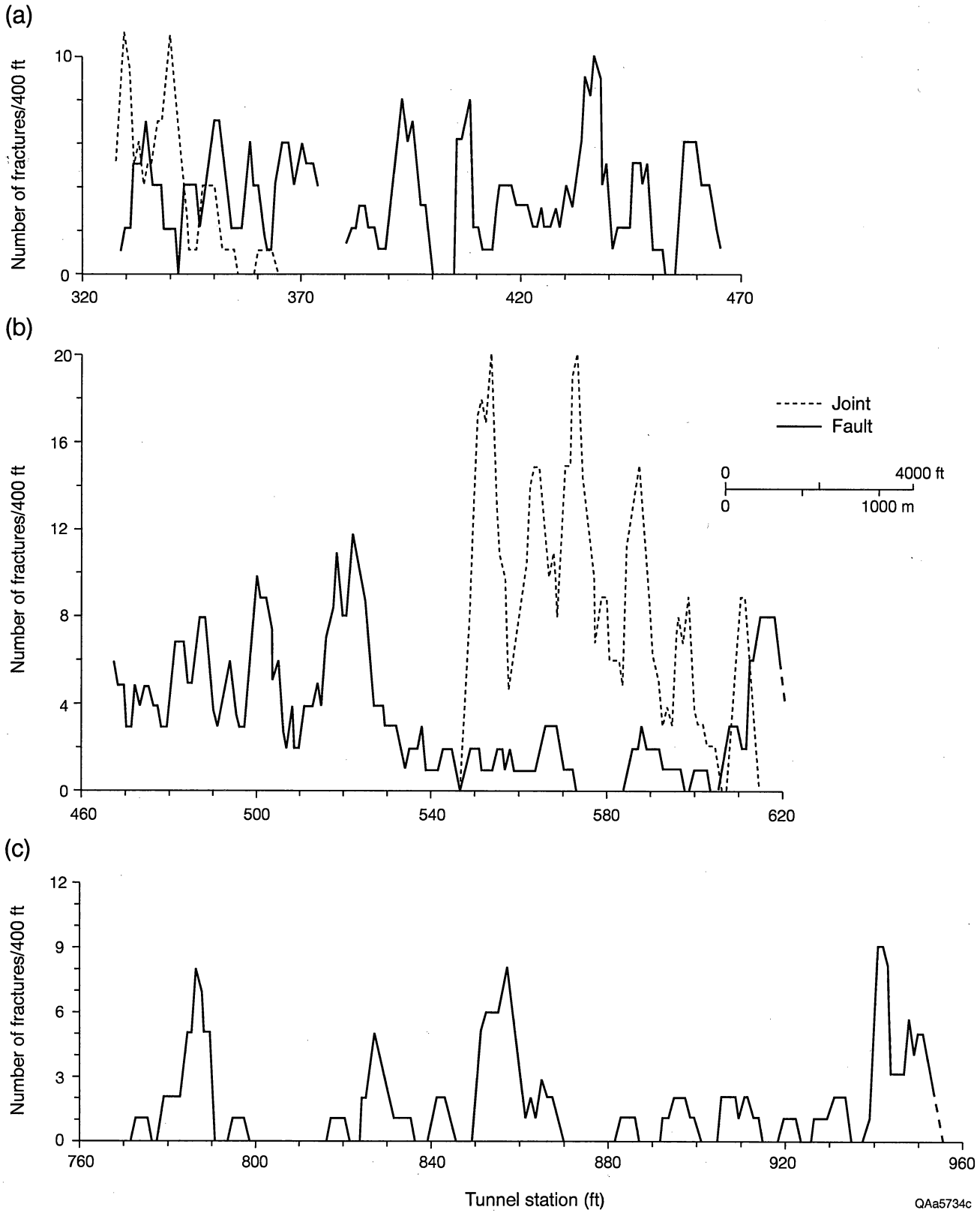

Figure 7. Graphs depicting fault and joint frequency on the basis of 400-ft running averages along tunnel segments: (a) N25–N30, (b) N30–N35+, and (c) N40–N45.3.

Table 2. Statistical summary of fractures in SSC tunnel sections in Austin Chalk.

Tunnel section	Type of fracture	Mean	Median	Standard deviation	Skewness	Number of points
			Strike			
N20–N35+	faults	334°	327°	±42°	0.832	244
N40–N45.3	faults	10°	13°	±43°	–0.435	79
N25–N30	joints	52°	50°	±8°	0.345	36
N30–N35+	joints	39°	40°	±7	–0.77	174
			Dip direction			
N20–N35+						
mode 1	faults	52°	51°	±33°	0.048	140
mode 2	faults	235°	233°	±44°	0.271	120
N40–N45.3						
mode 1	faults	98°	102°	±44°	–0.300	47
mode 2	faults	289°	286°	±34°	–0.315	36
			Dip			
All sections	faults	62°	61°	±12°	0.003	217
N25–N30	faults	62°	61°	±11°	–0.803	76
N30–N35+	faults	61°	60°	±12°	0.042	90
N40–N45.3	faults	62°	60°	±14°	0.175	41
			Throw (ft)			
All sections	faults[1]	–0.0036	0.0	±0.50	–0.015	257
All sections	faults[2]	0.99	1.00	0.31–3.14[3]	–	–
			Fracture Spacing			
N25–N30						
	faults[1]	1.64	1.72	±0.717	–0.400	113
	joints[1]	1.52	1.64	±0.730	–0.226	37
	faults[2]	44	53	8–228[3]	–	–
	joints[2]	33	44	6–178[3]	–	–
N30–N35+						
	faults[1]	1.53	1.58	±0.694	–0.203	160
	joints[1]	1.42	1.41	±0.390	0.29	173
	faults[2]	34	38	7–168[3]	–	–
	joints[2]	26	26	11–65[3]	–	–
N40–N45.3						
	faults[1]	1.67	1.63	±0.853	0.111	82
	faults[2]	47	43	7–333[3]	–	–

[1] Logarithm transformation of data
[2] Statistics retransformed standard length units (ft)
[3] Range shows ±1 standard deviation from mean

1992; Corbett et al., 1991; Friedman and Wiltschko, 1992; Friedman et al., 1994), but other attributes—particularly distribution patterns—differ significantly from those described at outcrop.

Faults

Normal faults are the most common structure in the SSC tunnels, as also noted in numerous shallow cores from near the SSC site (Collins et al., 1992). Approximately 350 faults were mapped over 9.4 mi of accumulated exposure. Fault throws are commonly small, ranging from less than 1 inch to more than 10 ft. Of the 257 faults for which throw was measured, half have throws of 1 ft or less (Table 2), 30 percent have throws of more than 2 ft, and 10 percent have throws greater than 5 ft (Appendix A). Only two faults have throws in excess of 20 ft. Faults with greatest throw display the most breccia and vein calcite and generally produce the most water.

Faults commonly have striations (slickensides) showing dip-slip motion. Fault dips range from about 45°–85°, having an average dip of approximately 60° (Table 2). Large faults are planar within the tunnel, but small faults are commonly slightly to strongly curved in both cross section and plan view (Figs. 3b, c, and 5). Where they cross chalk and marl beds, faults are often composed of steeply dipping segments (ramps) and shallowly dipping segments (flats). Faults generally flatten to dips of about 30° where they intersect marl beds 6 inches or more thick. Voids that developed near irregularities in fault profiles are the loci of wide calcite veins, fault breccia, antithetic faults, and water production.

Faults end against other faults (Fig. 3d), or offsets decrease to tip lines (Fig. 3a). In a few cases, throw diminishes by as much as 2 ft within a distance of 15 ft (Figs. 3a and 5). Small antithetic faults that have downdip terminations against larger faults are common (Fig. 3b). Small fault-bounded lenses that parallel fault zones are also common. Horst-and-graben patterns are evident in all tunnel segments, regardless of tunnel alignment azimuth (Fig. 3b).

Folds and Associated Faults

Austin Chalk bedding has uniform attitudes over long distances at the SSC site, and folds are uncommon. Three types of folds occur: distorted beds between fault planes or along fault surfaces ("drag folds" or marl "smears"; Fig. 5); rollover monoclines in fault hanging wall blocks (Figs. 3c and 5); and broad, low-relief monoclines and anticlines (Fig. 4).

Marl smears are 1- to 2-ft-long masses entrained along fault surfaces that taper from intact marl beds to a cutoff point along fault surfaces. Smears are most prominent where marl beds are more than 4 inches thick. Folds of this type are rarely more than a few feet wide.

Asymmetric monoclines (rollover folds) are located in adjacent hanging wall blocks of faults having throws of as little as 1 ft. Rollover folds have open hinges in which bed dips change gradually by approximately 5°–10°, having beds tilted down toward faults. Width of tilted bed zones in rollover folds ranges from 14 to 140 ft. Width does not correlate systematically with fault size, and wide rollovers are not necessarily associated with large faults. Rollover folds, many of which are inclined only a degree or two, occur in more than half of the faults having throws of 1 to 4 ft but are absent from faults with 9 ft or more of throw. For these large faults, rollover folds may be replaced with a wide area of tilted beds bounded by two inward-facing faults. Rollover folds could reflect accommodation of hanging wall rocks to an overall listric (downward-flattening) fault geometry, which is consistent with previous interpretations that large faults flatten in underlying Eagle Ford Shale (The Earth Technology Corporation, 1989). In most rollover folds associated with faults having throw of less than 4 ft, no additional joints or faults are present in fold hinges or tilted beds.

Open large-scale folds have wavelengths on the order of 4,500 ft or more and have northeastward axial trends. These are not rollover folds associated with large faults but small faults that occur locally within these folds. Two anticlines in N40–N45.3 (Fig. 4) have fault swarms on westward-dipping (5°) limbs. Both anticlines also have crestal grabens. The few faults found in the intensely jointed section of N30–N35+ are located on the limbs of a broad,

undulating monocline. Most faults observed at the SSC site, however, are in areas of homoclinal dip.

Joints

Joints at tunnel depths are single fractures or strands composed of en echelon segments. Joint segments are several inches to several feet long. Most joints dip slightly (~85°) to the northwest, orthogonally to southeast-dipping beds. The northeastward strike (Figs. 3f and 6d; Table 2) is subparallel to normal faults mapped at the surface (Fig. 6e). Joints occur as simple fractures or are coated or filled with calcite or, rarely, pyrite.

Joints in the tunnel commonly terminate against marl beds, a pattern also evident in outcrop. Although most joints are restricted to individual chalk beds, nearly coplanar joints are commonly stacked in adjacent chalk beds. Joint continuity is interrupted by intervening marl beds. Commonly, such stacked joints are separated laterally by a few inches even where separated vertically by several inches of marl. Fewer than 10 percent of joints end within chalk beds (Fig. 5).

Faults and joints are not necessarily coincident or parallel. Joints rarely occur together with faults, with few exceptions (Fig. 3a). Joints are most prominent in part of tunnel segment N30–N35+ where faults are less common, whereas the southern half of N30–N35+ has no joints but contains numerous faults. Previous outcrop observations suggested that large faults are surrounded by halos of joints (Collins et al., 1992). In contrast, tunnel faults are not surrounded by halos of joints. Instead, veins and small antithetic faults are localized near undulations in fault surfaces. Methods of using joint spacing in order to verify the existence of faults (Pohn, 1981; Wheeler and Dixon, 1980) would not be effective in this area. Where joints and faults occur together, joints abut faults and are not offset by them (Figs. 3a and 5), suggesting that joints postdate faults.

Long sections of the tunnel, including one that is 21,000 ft long in N25–N35+, lack joints entirely. Few joints occur in east–west-trending tunnel N40–N45.3 (over 19,000 ft long). Given

this tunnel heading, the scarcity of northeast-trending joints in this area cannot be attributed to sampling bias (discussed later). Prevalence of joints in outcrop may give a misleading view of joint density, as well as connectivity, at depths as shallow as 100 ft.

Ground-surface joint orientation patterns and other attributes differ from those of joints in tunnels. At ground surface, a northeast-striking set is dominant, but northwest-striking joints are also widespread, particularly in weathered rock or quarry exposures. The northwest-striking joint set is rare in the tunnel, suggesting that this set is restricted to depths of less than 100 ft. Joints at ground surface also commonly have strongly curved en passant joint terminations (Fig. 5), whereas segmented tunnel joints commonly have straight overlapping ends, possibly reflecting reactivation and growth of joints in the near-surface environment. Outcrop and near-surface fracture networks may thus be more interconnected than those at depth. Near-surface joints have solution-enhanced apertures and halos of bleached, oxidized rock that are absent in tunnel joints.

Fracture Swarms

Faults and joints in the SSC tunnel are arranged in swarms. Fracture-frequency diagrams that average fracture abundance over 400-ft intervals illustrate this pattern (Figs. 6f and 7). Small faults (throw <10 ft) generally occur in clusters or broad swarms that have as many as 24 faults and a maximum of 12 faults per 400 ft of tunnel length (Fig. 7a, b, c).

In some areas, spacing between fault swarms is several thousand feet. For example, within the 3.6-mi-long N40–N45.3 segment there are 4 swarms containing 5 to 10 faults that are spaced 3,000 to 9,000 ft apart. One 3,700-ft section between the two westernmost swarms is broken by only two small faults and two joints. Between the two easternmost swarms, one 7,000-ft-long reach has only one or two faults every thousand feet (Fig. 7c). In N25–N35+, preliminary interpretation of fault- and fault-size-frequency data suggests that small faults can be subdivided into 1,500- to 2,000-ft-wide swarms spaced about 2,000 ft apart and narrow swarms approximately 500 to 1,000 ft wide spaced about 800 to 1,000 ft apart (Fig. 7a, b). Fault

swarms are as much as 2,000 ft wide, and spacing between swarms ranges from 800 to 2,000 ft and averages about 1,000 ft.

Sections of tunnel as much as 21,000 ft long lack joints. Segments of the tunnel in which joints occur are arranged in swarms. Joint swarms containing as many as 25 joints are an average of 500 ft wide and 500 to 1,000 ft apart. Joints within swarms are spaced about 0.5 to 60 ft apart. Joints and joint swarms are much less common than faults (Fig. 7a, b). Swarms of faults and joints are not coincident or necessarily parallel, and faults are not surrounded by halos of joints.

Within fault swarms, fault frequency varies considerably, sometimes systematically. For example, fault frequency within each swarm in N30–N35+ decreases progressively from north to south (Fig. 7b). Fracture frequencies within joint swarms also vary systematically. In N30–N35+, joint frequency decreases northward and reaches lowest values near a major fault swarm near N35 (Fig. 7b). Joint density progressively decreases or increases from swarm to swarm near N25 (Fig. 7b). Moreover, systematic shifts in joint orientation are evident. In N30–N35+, average joint strike swings from about 023° at the southern limit of jointing to 049° near the northern limit. Within this overall trend, however, joint strikes swing 5°–10° between more northerly and more easterly strikes, forming domains defined by contrasting strike groupings that are spaced about 700 ft apart (Fig. 7f).

Sampling Bias

Northwest-trending faults dominate in northeast-trending tunnel segments and vice versa (Fig. 6a, b). The 16-ft-wide SSC tunnel is much narrower than the average spacing of fractures (tens to hundreds of feet). This fracture spacing creates a bias toward sampling fractures that strike at high angles to the tunnel axis. Apparent fracture spacing along a traverse across evenly fractured areas increases as trend of traverse and fractures becomes increasingly similar (Hudson and Priest, 1983; LaPointe and Hudson, 1985). The SSC tunnel curves from parallel to perpendicular to regional fault strike. The resulting sampling bias may account for contrasts in

abundance of northwest- and northeast-striking faults in different tunnel segments. By factoring in sampling bias that favors encountering fractures that strike across the tunnel and by correcting for bias due to different tunnel lengths along and across fault strikes, we calculate that northwest-trending faults dominate and that a population of northeast-trending faults is less common (Fig. 6c). Fault- and joint-spacing patterns are not explained by sampling bias, however, and are real attributes of deformation along tunnel segments where they are measured.

Water Flow

Qualitative estimates of water production from faults ranged from dry, damp, or dripping, to flowing at rates of 200 to 300 gallons per minute (Jim Carroll, SSC Laboratory, personal communication, 1994). A few joints produced trace amounts of water; copious water flow from joints was not observed. Several visits to water-productive areas over a six-month period showed that water production from fractures decreased with time after excavation. Water continued to drain from only a few large faults and some joints after more than six months. In faults, water drained from brecciated or veined zones of widely varying widths. Tens of gallons of water per minute were produced from a single, approximately 2-ft by 4-inch cavity in a fault zone near N35 (Figs. 2 and 3g). Other faults and joints in this zone were dry. Only parts of fault swarms and parts of individual fault planes thus transmit fluid.

IMPLICATIONS

This paper describes the types of structural data collected at the SSC site. SSC tunnel fracture maps provide an unrivaled view of small-scale faults and joints within a regional normal fault zone. Although this report presents only a preliminary analysis of this data set, it is clear that observations in the SSC tunnel will provide new insight into spacing and size distribution of faults and joints that can be used to improve structural models and guide interpretation of

conventional borehole and outcrop data. For example, none of the nonlinear joint-spacing/bed-thickness distributions commonly accepted and used in engineering applications (for example, Huang and Angelier, 1989) are appropriate for subsurface Austin Chalk at the SSC site. Instead, joints and faults are in swarms spaced approximately 1,000 ft apart. Although little information is available concerning fracture-swarm spacing versus brittle-bed thickness for chalk, we speculate that fault-swarm spacing is a function of the thickness of the entire Austin Chalk (about 500 ft at the SSC site; Fig. 8) and that proportionately wider fault-swarm spacing will be found in areas such as Giddings field where Austin Chalk is thicker than at the SSC site.

Faults and joints, including those in Austin Chalk, are targets for horizontal drilling in the petroleum industry (Kuich, 1990; Stark, 1992). Although Ellis County tunnel exposures are more than 150 mi north of major producing areas of Austin Chalk in Pearsall and Giddings fields (Galloway et al., 1983), many aspects of structure and stratigraphy resemble those of major Austin Chalk fields. Minor amounts of oil have been produced from fractured Austin Chalk in a small field 36 mi south of the study area (Hood, 1951). Analysis of fracture maps from the SSC site is likely to be germane to existing and new areas of chalk hydrocarbon production and to other mildly extended rocks where fracture swarms are conduits for fluid flow.

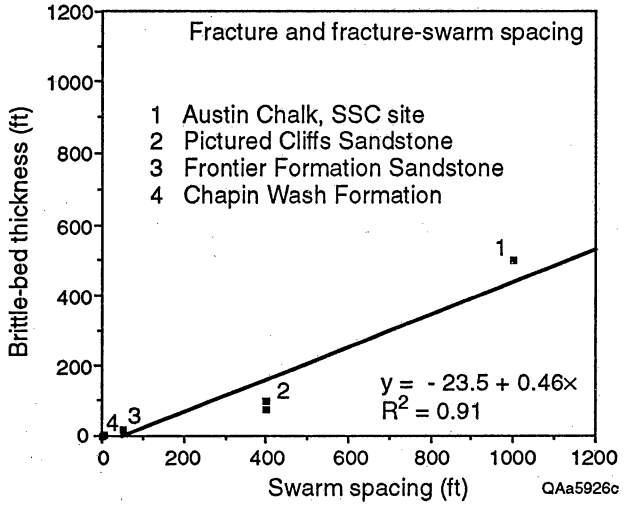

Figure 8. Fracture and fracture-swarm spacing versus brittle-bed thickness. Brittle-bed thickness for Austin Chalk = formation thickness. Pictured Cliffs and Frontier Formation sandstone data from Laubach (1992); Chapin Wash Formation sandstone data in part from Laubach et al. (1991).

ACKNOWLEDGMENTS

Publication authorized by the Director, Bureau of Economic Geology. We thank E. W. Collins, S. D. Hovorka, K. Schroeder, and C. Smith for assistance in tunnel mapping and Robert E. Mace for statistical analysis of fractures. We also thank E. W. Collins, T. F. Hentz, S. D. Hovorka, and P. P. Nelson for reviews. This study was funded by the Texas National Research Laboratory Commission (TNRLC) under interagency contract IAC(92-93)-0301.

REFERENCES

Collins, E. W., 1987, Characterization of fractures in limestone, northern segment of the Edwards aquifer and Balcones Fault Zone, Central Texas: Gulf Coast Association of Geological Societies Transactions, v. 37, p. 43–54.

Collins, E. W., Hovorka, S. D., and Laubach, S. E., 1992, Fracture systems of the Austin Chalk, North-Central Texas, *in* Schmoker, J. W., Coalson, E. B., and Brown, C. A., eds., Geological studies relevant to horizontal drilling: examples from western North America: Rocky Mountain Association of Geologists, p. 129–142.

Collins, E. W., and Laubach, S. E., 1990, Faults and fractures in the Balcones Fault Zone, Austin region, Central Texas: Austin Geological Society Guidebook 13, 34 p.

Corbett, K. P., Friedman, M., Wiltschko, D. V., and Hung, J. H., 1991, Controls on fracture development, spacing, and geometry in the Austin Chalk Formation, Central Texas: consideration for exploration and production: Dallas Geological Society Field Trip Guidebook, 49 p.

Friedman, M., Kwon, O., and French, V., 1994, Experiments and field observations of containment of fractures within brittle beds of the Austin Chalk, *in* Nelson, P. P., and

Laubach, S. E., eds., Rock mechanics: models and measurements/challenges from industry, Proceedings, First North American Rock Mechanics Symposium: Rotterdam, The Netherlands, Balkema, p. 833–842.

Friedman, M., and Wiltschko, D. V., 1992, An approach to exploration for naturally fractured reservoirs, with examples from the Austin Chalk, *in* Schmoker, J. W., Coalson, E. B., and Brown, C. A., eds., Geological studies relevant to horizontal drilling: examples from western North America: Rocky Mountain Association of Geologists, p. 143–153.

Galloway, W. E., Ewing, T. E., Garrett, C. M., Tyler, Noel, and Bebout, D. G., 1983, Atlas of major Texas oil reservoirs: The University of Texas at Austin, Bureau of Economic Geology, 139 p.

Gilchriese, M. G. D., and Metropolis, K., 1990, Site-specific conceptual design of the Superconducting Super Collider Laboratory: Report No. SSCL-SR-1055, 59 p.

Hood, F. W., 1951, Mount Calm Field, *in* Herald, F. A., ed., Occurrence of oil and gas in northeast Texas: University of Texas, Austin, Bureau of Economic Geology Publication No. 5116, 449 p.

Hovorka, S. D., and Nance, H. S., in press, Dynamic depositional and early diagenetic processes in a deep-water shelf setting, Upper Cretaceous Austin Chalk, North Texas: Gulf Coast Association of Geological Societies Transactions, v. 44.

Huang, Q., and Angelier, J., 1989, Fracture spacing and its relation to bed thickness: Geological Magazine, v. 126, no. 4, p. 355–362.

Hudson, J. A., and Priest, S. D., 1983, Discontinuity frequency in rock masses: International Journal of Rock Mechanics and Mining Sciences & Geomechanics Abstracts, v. 20, no. 2, p. 73–89.

Kuich, N., 1990, Seismic fracture identification and horizontal drilling: keys to optimizing productivity in a fractured reservoir, Giddings field, Texas: Gulf Coast Association of Geological Societies Transactions, v. 39, p. 153–158.

LaPointe, P. R., and Hudson, J. A., 1985, Characterization and interpretation of rock mass joint patterns: Geological Society of America, Special Paper 199, 37 p.

Laubach, S. E., 1992, Fracture networks in selected Cretaceous sandstones of the Green River and San Juan Basins, Wyoming, New Mexico, and Colorado, *in* Schmoker, J. W., Coalson, E. B., and Brown, C. A., eds., Geological studies relevant to horizontal drilling in western North America: Rocky Mountain Association of Geologists, p. 61–74.

Laubach, S. E., Hamlin, H. S., Buehring, R., Baumgardner, R. W., Jr., and Monson, E. R., 1990, Application of borehole-imaging logs to geological analysis, Cotton Valley Group and Travis Peak Formation, GRI Staged Field Experiment wells, East Texas: The University of Texas at Austin, Bureau of Economic Geology, topical report prepared for the Gas Research Institute under contract no. 5082-211-0708, 115 p.

Laubach, S. E., Vendeville, B. C., and Reynolds, S. J., 1991, Patterns in the development of extensional fault-block shapes from comparison of outcrop-scale faults and experimental physical models, *in* Larsen, R. M., Brekke, H., Larsen, B. T., and Talleraas, E., eds., Structural and tectonic modeling and its application to petroleum geology: Norwegian Petroleum Society Special Publication No. 1, p. 95–101.

McGowen, J. H., Proctor, C. V., Haenggi, W. T., Reaser, D. F., and Barnes, V. E., 1987, Dallas Sheet, *in* Barnes, V. E., Geologic atlas of Texas: The University of Texas at Austin, Bureau of Economic Geology, scale 1:250,000.

Nance, H. S., 1993, Geologic mapping of fractures and faults in the SSC surface excavations and tunnels: The University of Texas at Austin, Bureau of Economic Geology, interim data

report prepared for Texas National Research Laboratory Commission under contract no. IAC(92-93)-0301, 8 p. plus appendices.

Nelson, P. P., 1993, TBM performance analysis with reference to rock properties (Chapter 10, v. 4), *in* Hudson, J. A., ed., Comprehensive rock engineering: Oxford, United Kingdom, Pergamon Press, p. 261–291.

Pohn, H. A., 1981, Joint spacing as a method for locating faults: Geology, v. 9, p. 258–261.

Reaser, D. F., and Collins, E. W., 1988, Style of faults and associated fractures in Austin Chalk, northern extension of the Balcones Fault Zone, Central Texas: Gulf Coast Association of Geological Societies Transactions, v. 38, p. 267–276.

Stark, P. H., 1992, Perspectives on horizontal drilling in Western North America, *in* Schmoker, J. W., Coalson, E. B., and Brown, C. A., eds., Geologic studies relevant to horizontal drilling: examples from western North America: Rocky Mountain Association of Geologists, p. 3–14.

The Earth Technology Corporation, 1989, Bedrock geology of the Superconducting Super Collider site: The Earth Technology Corporation, Report SSC-GR No. 65.

Wheeler, R. L., and Dixon, J. M., 1980, Intensity of systematic joints: methods and application: Geology, v. 8, p. 230–233.

Appendix A. Fault orientation data from SSC tunnel sections.

Tunnel segment	Location (ft)	Strike (degrees)	Dip (degrees)	Dip direction (degrees)	Average throw (ft)
N20–N25	27030	084	71.4	354	nd
	27119	281	72.7	191	nd
	27244	274	57.9	184	nd
	27578	333	75.0	063	nd
	27784 to	31170: cc*			
	31403	316	59.4	046	nd
	31422	312	83.4	042	nd
	31460	294	55.4	024	nd
	31475	290	77.7	200	nd
	31481	285	71.6	015	nd
	31489	283	71.6	013	nd
N25–N30	32643	009	29.3	099	1.50
	33092	297	64.7	027	1.00
	33101	327	68.1	057	1.08
	33340	305	64.2	215	1.75
	33345	287	46.4	197	0.50
	33381	271	53.9	001	0.25
	33529	008	nt	098	0.75
	33542	283	51.6	193	1.50
	33612	292	72.0	022	2.00
	33615	348	nt	258	1.00
	33921	314	56.6	044	4.50
	33924	288	60.3	198	0.13
	34467	328	88.7	058	0.18
	34471	301	nt	031	5.00
	34472	301	64.1	211	1.00
	34479	315	59.6	225	0.50
	34888	053	89.5	323	0.25
	34894	075	68.4	345	1.25
	34964	322	56.5	232	1.00
	35009	005	nt	095	0.50
	35048	335	60.7	065	0.63
	35075	320	59.7	230	1.75
	35180	273	60.4	183	1.50
	35261	082	nt	172	0.18
	35271	276	51.3	006	0.75
	35621	319	60.9	049	2.50
	35640	282	64.7	192	1.25
	35882	068	nt	158	1.13
	35888	075	36.9	165	0.50
	35979	295	44.8	025	1.25
	35985	326	nt	056	2.00
	36314	271	70.5	181	0.75
	36529	341	nt	251	0.50
	36549	326	76.2	056	1.50
	36579	292	46.0	202	2.25
	36800	316	71.6	046	3.25

nt = fault does not extend across exposure
nd = average not determined
*cc = concrete covered

Appendix A (cont.)

Tunnel segment	Location (ft)	Strike (degrees)	Dip (degrees)	Dip direction (degrees)	Average throw (ft)
N25–N30 (cont.)	36907	344	63.5	074	1.25
	37027	340	56.3	250	1.75
	37072	299	61.6	209	1.25
	37128	354	59.1	264	3.00
	37328	299	61.5	209	2.00
	37437 to	38154: cc*			
	38166	337	45.2	067	2.00
	38229	275	53.4	185	5.50
	38434	346	73.3	256	1.75
	38574	272	81.2	002	0.25
	38575	352	63.8	262	0.75
	38962	323	57.5	233	3.00
	39178	057	nt	147	1.75
	39218	335	83.1	245	1.50
	39368	345	57.8	075	0.50
	39395	283	75.1	013	1.75
	39445	286	59.6	016	4.50
	39617	353	54.8	083	1.00
	39644	011	nt	101	0.25
	39661	304	60.1	214	0.25
	40634	304	57.8	034	1.50
	40646	311	53.1	041	1.50
	40661	316	nt	046	nd
	40663	315	nt	045	nd
	40664	315	70.6	225	>9
	40686	358	nt	268	5.00
	40841	348	nt	078	1.50
	40910	316	nt	046	3.50
	41311	338	67.0	068	2.00
	41530	327	72.9	237	3.25
	41650	327	nt	237	4.00
	41690	304	nt	214	4.00
	41765	040	nt	310	nd
	41825	031	nt	121	nd
	41930	298	nt	028	5.25
	42028	016	80.1	286	nd
	42057	040	nt	310	nd
	42240	273	59.0	183	5.75
	42474	310	71.3	220	4.00
	42526	326	71.1	056	2.25
	42846	301	50.9	031	3.00
	42888	332	57.7	242	2.25
	43023	348	68.6	258	1.50
	43194	314	59.9	224	1.75
	43294	303	60.6	033	5.00
	43386	313	68.9	043	1.00
	43394	319	70.2	049	1.50
	43446	310	81.2	040	0.70

Appendix A (cont.)

Tunnel segment	Location (ft)	Strike (degrees)	Dip (degrees)	Dip direction (degrees)	Average throw (ft)
N25–N30 (cont.)	43467	335	46.2	065	3.00
	43508	320	nt	050	0.50
	43518	310	nt	040	nd
	43530	285	70.4	015	0.50
	43532	283	nt	193	nd
	43572	038	nt	308	0.50
	43740	310	nt	220	nd
	43742	356	42.3	266	1.75
	43746	345	nt	255	0.25
	43758	272	nt	182	0.13
	44056	321	56.1	051	1.00
	44283	328	56.4	058	2.50
	44494	271	74.1	001	4.00
	44533	011	nt	281	0.50
	44615	287	nt	017	nd
	44657	072	64.5	162	5.00
	44662	296	nt	206	0.50
	44685	348	57.8	078	2.00
	44903	307	nt	037	0.25
	44910	340	77.7	070	1.00
	45683	315	nt	045	0.50
	45692	318	44.5	048	1.00
	45708	316	60.9	040	1.00
	45714	333	nt	063	0.18
	45719	333	65.4	063	0.38
	45722	331	nt	241	1.00
	45952	072	nt	342	0.38
	46030	048	nt	138	1.00
	46095	318	65.3	048	3.00
	46098	294	nt	024	0.25
	46186	328	61.2	058	4.25
N30–N35	46537	354	88.6	084	3.00
	46639	275	nt	185	0.50
	46763	311	69.3	041	6.00
	46782	302	65.3	212	2.00
	46812	353	60.9	083	1.00
	46815	350	71.0	260	0.17
	47054	012	63.9	102	4.50
	47172	345	65.0	075	1.40
	47258	291	82.9	201	2.00
	47332	274	49.0	004	2.75
	47388	024	37.2	294	2.00
	47536	082	69.2	352	2.50
	47571	329	48.0	059	2.00
	47615	001	nt	091	1.75
	47716	346	53.7	076	2.00
	47970	078	79.9	168	0.70
	48007	299	64.8	029	1.00

Appendix A (cont.)

Tunnel segment	Location (ft)	Strike (degrees)	Dip (degrees)	Dip direction (degrees)	Average throw (ft)
N30–N35 (cont.)	48106	298	58.7	028	1.00
	48195	349	54.0	259	1.90
	48272	336	62.6	246	1.00
	48280	320	45.2	230	2.80
	48286	321	nt	231	1.00
	48354	335	79.3	245	3.00
	48434	006	57.4	096	0.50
	48435	071	nt	161	0.20
	48455	286	nt	196	0.25
	48612	345	nt	105	0.50
	48616	355	58.4	095	0.90
	48671	335	61.4	245	1.00
	48704	051	nt	321	0.70
	48814	280	52.8	010	9.00
	48821	322	nt	052	1.00
	48850	312	69.6	222	0.40
	49100	314	67.4	224	1.50
	49225	052	nt	142	0.17
	49230	320	70.0	230	1.50
	49252	025	77.2	115	2.25
	49264	322	nt	052	0.17
	49366	035	75.3	305	3.00
	49405	052	nt	322	0.20
	49464	327	67.7	057	5.00
	49468	077	nt	347	0.40
	49470	085	nt	355	0.40
	49508	304	45.8	034	1.25
	49855	033	59.2	123	1.00
	49889	334	78.6	064	5.00
	49914	358	36.9	268	3.00
	49922	308	57.1	218	6.00
	49946	288	nt	018	0.75
	49954	287	68.4	017	1.50
	49960	066	nt	156	0.50
	50026	015	80.7	285	0.50
	50080	053	66.0	323	1.50
	50108	278	nt	008	2.25
	50116	322	nt	052	0.25
	50138	027	nt	117	2.25
	50164	054	nt	324	0.25
	50258	335	45.6	245	3.00
	50306	001	nt	271	0.40
	50354	295	49.4	025	2.50
	50394	313	45.1	043	0.40
	50429	323	nt	233	0.25
	50674	349	nt	079	0.40
	50681	318	49.8	048	2.00
	50694	345	52.0	255	1.00

Appendix A (cont.)

Tunnel segment	Location (ft)	Strike (degrees)	Dip (degrees)	Dip direction (degrees)	Average throw (ft)
N30–N35 (cont.)	50952	359	81.5	089	3.00
	51001	358	39.0	268	1.15
	51274	331	56.9	061	1.25
	51276	358	nt	268	0.40
	51283	352	nt	082	0.17
	51284	325	nt	055	0.17
	51286	055	nt	325	0.17
	51400	326	nt	236	0.17
	51402	325	nt	235	0.25
	51404	327	nt	237	0.10
	51405	293	79.7	023	6.50
	51410	306	47.9	216	0.75
	51596	008	nt	098	0.20
	51611	002	48.6	092	2.00
	51710	286	nt	196	0.15
	51722	376	nt	106	0.25
	51760	326	nt	046	0.25
	51802	341	52.3	251	0.33
	51820	294	81.8	024	0.75
	51879	293	52.7	023	0.70
	51969	316	nt	046	0.16
	52024	346	62.0	076	2.00
	52027	346	nt	256	0.25
	52037	347	75.3	283	1.75
	52051	327	nt	057	0.17
	52059	352	64.8	082	0.50
	52186	018	30.2	288	0.17
	52199	350	nt	080	0.17
	52233	312	57.3	042	1.00
	52293	285	56.3	195	2.75
	52303	285	nt	195	0.50
	52367	311	nt	221	0.50
	52378	012	nt	282	0.17
	52381	355	nt	265	0.17
	52384	057	nt	147	0.17
	52395	306	78.6	036	5.50
	52413	345	44.3	255	0.50
	52433	057	nt	327	0.50
	52462	327	66.4	057	0.10
	52480	298	nt	208	0.17
	52628	032	72.1	122	1.75
	52766	306	53.8	216	6.25
	52778	082	nt	172	1.00
	52886	282	65.1	192	1.50
	53009	328	nt	238	0.25
	53148	272	60.1	182	1.50
	53155	355	nt	085	0.75
	53194	058	nt	328	0.17

Appendix A (cont.)

Tunnel segment	Location (ft)	Strike (degrees)	Dip (degrees)	Dip direction (degrees)	Average throw (ft)
N30–N35 (cont.)	53224	013	nt	103	1.25
	53233	025	nt	115	0.17
	53659	284	49.0	194	0.75
	53675	—	nt	240	nd
	53695	359	49.1	089	0.50
	53738	283	nt	193	0.10
	53904	346	71.4	076	8.50
	54034	329	nt	239	0.33
	54043	329	nt	239	0.17
	54058	270	nt	180	0.17
	54070	330	nt	060	0.33
	54144	327	nt	057	0.33
	54161	059	nt	329	0.20
	54495	281	50.7	191	1.00
	54981	343	50.3	073	5.00
	55050	332	57.3	242	0.50
	55051	332	nt	062	0.13
	55498	287	83.9	017	1.50
	55624	017	65.7	287	5.00
	55996	315	71.4	045	3.00
	56314	321	57.4	231	0.90
	56698	319	66.5	049	0.60
	56748	271	nt	001	1.00
	56780	334	63.0	244	1.50
	56787	—	nt	063	0.50
	57094	297	68.6	207	3.50
	58680	301	nt	211	1.25
	58783	318	59.4	228	3.50
	58786	—	nt	—	0.10
	58906	296	42.7	206	1.50
	59192	320	47.5	050	5.00
	59535	336	60.4	246	7.00
	60152	295	51.3	025	0.90
	60882	292	56.1	022	1.25
	60923	283	57.2	013	2.00
	60973	311	71.1	041	1.70
	61376	070	nt	160	3.00
	61401	345	74.5	075	37.00
	61406	330	48.1	240	10.00
	61414	352	41.3	262	10.00
	61415	348	62.0	258	10.00
N35–N35+	61710	295	nt	205	nd
	61716	299	nt	209	nd
	61722	290	nt	200	nd
	61835	343	nt	253	nd
	61838	010	nt	100	nd
	61841	340	nt	250	nd
	61847	001	nt	091	nd

Appendix A (cont.)

Tunnel segment	Location (ft)	Strike (degrees)	Dip (degrees)	Dip direction (degrees)	Average throw (ft)
N35–N35+ (cont.)	61859	347	nt	077	nd
	61865	004	nt	274	nd
	61889	022	nt	292	nd
N40–N45	76280	272	75.5	182	nd
	77463	359	51.4	089	nd
	78097	007	60.4	277	nd
	78099	017	50.3	287	nd
	78468	037	nt	127	nd
	78474	066	nt	156	nd
	78476	037	nt	127	nd
	78480	036	81.9	306	nd
	78488	020	nt	110	nd
	78496	047	57.9	317	nd
	78581	063	66.9	153	nd
	78679	047	56.1	137	nd
	78693	060	47.8	150	nd
	78811	002	62.1	092	nd
	78847	048	71.2	138	nd
	78853	029	43.6	299	nd
	78860	022	33.7	292	nd
	78889	046	89.4	316	nd
	81905	321	54.4	051	nd
	82626	026	41.9	296	nd
	82738	271	84.2	181	nd
	82873	280	59.6	010	nd
	82916	291	86.5	021	nd
	82972	281	86.7	011	nd
	83404	327	64.2	237	nd
	84288	298	68.0	028	nd
	84361	312	45.7	042	nd
	85252	014	nt	104	nd
	85262	104	nt	194	nd
	85284	069	nt	159	nd
	85295	031	nt	121	nd
	85318	014	nt	104	nd
	85341	012	nt	102	nd
	85383	344	52.0	254	nd
	85406	311	71.8	041	nd
	85672	044	48.8	134	nd
	85678	354	42.5	084	nd
	85728	017	47.1	107	nd
	85731	350	59.2	080	nd
	85795	066	68.6	336	nd
	85830	033	57.7	123	nd
	85835	015	nt	105	nd
	85850	042	64.5	312	nd
	85962	015	56.1	285	nd
	86103	015	66.4	285	nd

Appendix A (cont.)

Tunnel segment	Location (ft)	Strike (degrees)	Dip (degrees)	Dip direction (degrees)	Average throw (ft)
N40–N45 (cont.)	86425	013	60.4	103	nd
	86623	339	73.2	249	nd
	86716	344	69.8	254	nd
	88428	012	85.6	282	nd
	89470	349	72.8	259	nd
	89677	345	71.5	075	nd
	89838	327	50.9	237	nd
N45–N45+	90708	034	nt	124	nd
	90772	002	nt	092	nd
	91058	353	nt	263	nd
	91223	010	nt	100	nd
	92152	037	nt	307	nd
	92869	339	nt	249	nd
	93281	296	nt	026	nd
	93293	295	nt	025	nd
	94062	081	nt	351	nd
	94126	042	nt	312	nd
	94148	028	nt	298	nd
	94180	035	nt	125	nd
	94186	053	nt	143	nd
	94191	055	nt	145	nd
	94199	050	nt	140	nd
	94205	052	nt	322	nd
	94217	006	nt	276	nd
	94247	004	nt	094	nd
	94263	041	nt	131	nd
	94268	002	nt	092	nd
	94270	002	nt	092	nd
	94610	346	nt	076	nd
	94612	007	nt	277	nd
	94622	010	nt	280	nd
	94896	333	nt	063	nd
	94903	333	nt	063	nd
	94905	061	nt	151	nd
	94906	013	nt	283	nd
	94917	074	nt	344	nd
	95051	044	nt	314	nd
	95169	085	nt	355	nd

Appendix B. Joint orientation data from SSC tunnel sections.

Location (ft)	Strike (degrees)
N25–N30	
32513	057
32522	055
32585	071
32825	043
32954	060
32966	057
32972	056
32981	056
33043	049
33049	040
33101	—
33103	049
33125	041
33169	050
33191	048
33443	050
33481	044
33485	046
33487	046
33489	047
33549	—
33561	063
33562	063
33619	061
33836	040
33890	044
33963	058
33973	057
33983	058
34021	067
34099	061
34125	052
34245	050
34606	050
34840	040
35015	048
35376	040
36190	043
37437 to	38154: cc*
N30–N35	
54315	037
54363	024
54372	027
54390	038
54410	040
54482	030
54531	015
54815	028
54855	028
54863	021
54908	040
54926	047
54936	045
54992	030
55002	037
55010	035
55056	030
55092	038
55161	034
55188	041
55206	036
55246	034
55252	028
55261	033
55270	030
55277	033
55300	026
55318	012
55341	027
55362	036
55371	044
55381	039
55407	041
55461	040
55485	037
55493	024
55499	037
55521	038
55533	039
55570	035
55576	028
55656	023
55721	042
55728	036
55757	030
55799	024
55831	036
55896	040
56039	029
56067	031
56099	027
56111	032
56143	038
N30–N35	
56204	040
56251	042
56281	044
56338	039
56374	042
56402	040
56424	040
56435	032
56469	029
56475	034
56519	043
56547	044
56567	033
56595	033
56602	034
56623	038
56635	037
56652	040
56660	041
56704	024
56851	043
56871	038
56876	042
56916	046
56935	038
56947	033
56959	037
56965	034
56989	042
57021	041
57123	043
57134	039
57157	035
57180	037
57197	041
57222	036
57246	035
57264	040
57278	042
57290	044
57304	035
57323	038
57339	039
57355	045
57369	035
57404	041
57407	031

*cc = concrete covered

Location (ft)	Strike (degrees)	Location (ft)	Strike (degrees)
N30–N35		N30–N35	
57414	039	59722	047
57462	042	59747	035
57479	046	59768	045
57501	049	59790	046
57543	026	59800	047
57549	027	59826	034
57561	025	59899	047
57593	021	59950	045
57706	042	60080	045
57738	041	60095	049
57777	043	60350	031
57816	041	60402	037
57845	051	61032	050
57881	041	61062	049
57938	044	61070	047
58071	043	61104	030
58078	037	61128	048
58123	046	61132	044
58141	042	61155	039
58188	046	61209	045
58332	045	61227	044
58403	045	61241	044
58474	047	61328	047
58510	048	61340	038
58578	047	61355	036
58633	045	61373	037
58650	042	61430	036
58703	045		
58709	044		
58745	045		
58810	043		
58851	054		
58873	044		
58905	043		
58911	046		
58924	047		
58981	043		
59042	043		
59077	046		
59107	042		
59131	043		
59155	050		
59266	047		
59341	048		
59369	050		
59541	049		
59657	044		